Introduction

Purely acoustic wave propagation, typically including the effects of anisotropy and attenuation, is widely used for commercial full-waveform inversion of marine seismic data. In a wide range of circumstances, acoustic FWI has proven to be a good commercial compromise between computational cost and geophysical accuracy. However, the real world is elastic, and in some less-usual circumstances, elastic effects can render the results of acoustic FWI unreliable. Although fully elastic FWI of marine data is practical in some circumstances, low shear-wave velocities close to the seabed make true elastic FWI unfeasibly expensive in many areas. It is common for seabed shear velocities to be less than a few hundred metres per second, and in some extreme areas, they can be only a few tens of metres a second. Such low shear velocities mean that the computational cost of conventional 3D full-elastic FWI is orders of magnitude higher than acoustic FWI, and so can be beyond even the deepest pockets of most companies.

Here, we tackle a shallow-water dataset that contains strong elastic effects that damage conventional acoustic FWI. We do this using machine learning to build an equivalent acoustic dataset from an observed elastic field dataset, and to build an equivalent elastic dataset from a simulated acoustic dataset. The former allows us to undertake acoustic FWI effectively on elastically affected field data, and the latter allows us to undertake elastic FWI on a field dataset at a cost that is comparable to that of acoustic FWI. We achieve this using a supervised CycleGAN algorithm to train two networks to perform forward and reverse mapping between acoustic and elastic data using paired synthetic data, and a subset of the field data, subsequently applying the trained network to the entire field dataset.

Methodology

A CycleGAN is a cycled generative adversarial network, proposed by Zhu et al. (2017) as an effective deep-learning architecture for 2D image-domain translation. It has been widely used, in unsupervised mode, to map between, for example, day-time and night-time images, or satellite photographs and conventional street maps. Here, we use it supervised to map between 2D slices taken through acoustic and elastic shot records. We have available both elastic field data, and paired elastic and acoustic synthetic data; together these inputs are sufficient to train a supervised CycleGAN to convert elastic to acoustic data, and vice versa.

Assuming an acoustic data domain A and an elastic data domain E, the CycleGAN builds a generator $G : A \rightarrow E$ which translates data from its acoustic form to the elastic domain, and a coupled inverse generator $F : E \rightarrow A$ which translates in the opposite direction. For each mapping, an adversarial discriminator D is trained together with the generator to ensure the distribution of the output of the generator is indistinguishable from the distribution of the real data in the corresponding domain in the low-level feature space (Hoffman et al., 2017). Besides the adversarial loss, the CycleGAN also implements a cycle-consistency loss $F(G(A)) \approx A$, and an identity loss $F(A) \approx A$, during the training processes. These two terms are crucial to guarantee the effectiveness, robustness and performance of the generators. In our implementation, to ensure that the output of the generator is suitably accurate for seismic inversion, we train the networks with paired data and apply an extra L_1 loss between the generator output and the desired real seismic data to reduce the matching error between them. By comparing the performances of a variety of generator architectures, we have found that a 9-block ResNet (He et al., 2016) produces the most accurate outputs.

We have applied this approach to a dataset from the UKCS that contains shallow over-compacted chalk lying beneath low shear-velocity clastics. The strong shear contrast at top chalk in this dataset leads to strong p-s conversions in the field data, whereas the absence of conversions in acoustic modelling means that post-critical p-wave reflections, and their strong surface multiples, are visible in acoustic synthetic data but are not visible in the field data. Consequently, acoustic FWI fairs poorly on this dataset below top chalk. Figure 1 illustrates this; the strong acoustic wide-angle reflections and multiples at top chalk are supressed during FWI by eliminating the chalk layer from the model.

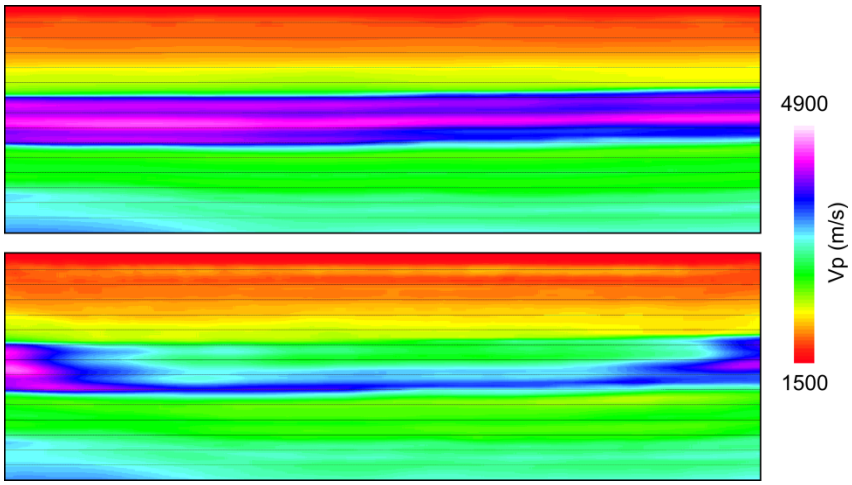

Figure 1 *Vertical slice through the velocity model. Top chalk is at about 1 km depth here.*

Top: tomography model.

Bottom: FWI model; the fast chalk layer has been removed by acoustic FWI.

Results

The training set consists of 5,000 paired shot records, randomly selected from a total of 100,000 pairs of inline shot records so that only 5% of the available field data are used for training. Before training, amplitudes were normalised between ±1, and the data were augmented by randomly low-pass filtering at frequencies between 3 and 10 Hz to make the network aware of different frequency bands.

Figure 2 shows results part way through the training process. The *Real Acoustic* and *Real Elastic* data are paired synthetic shot records based upon the field data. The acoustic data show strong reflections from top chalk, while the elastic data do not. The *Fake Acoustic* and *Fake Elastic* data show the output of the generator networks. The fake datasets should match their real counterparts. The *Recovered* and *Identity* records are also compared with the real records to train the generators via inclusion of cycle-consistency and identity losses; these should also match their real counterparts.

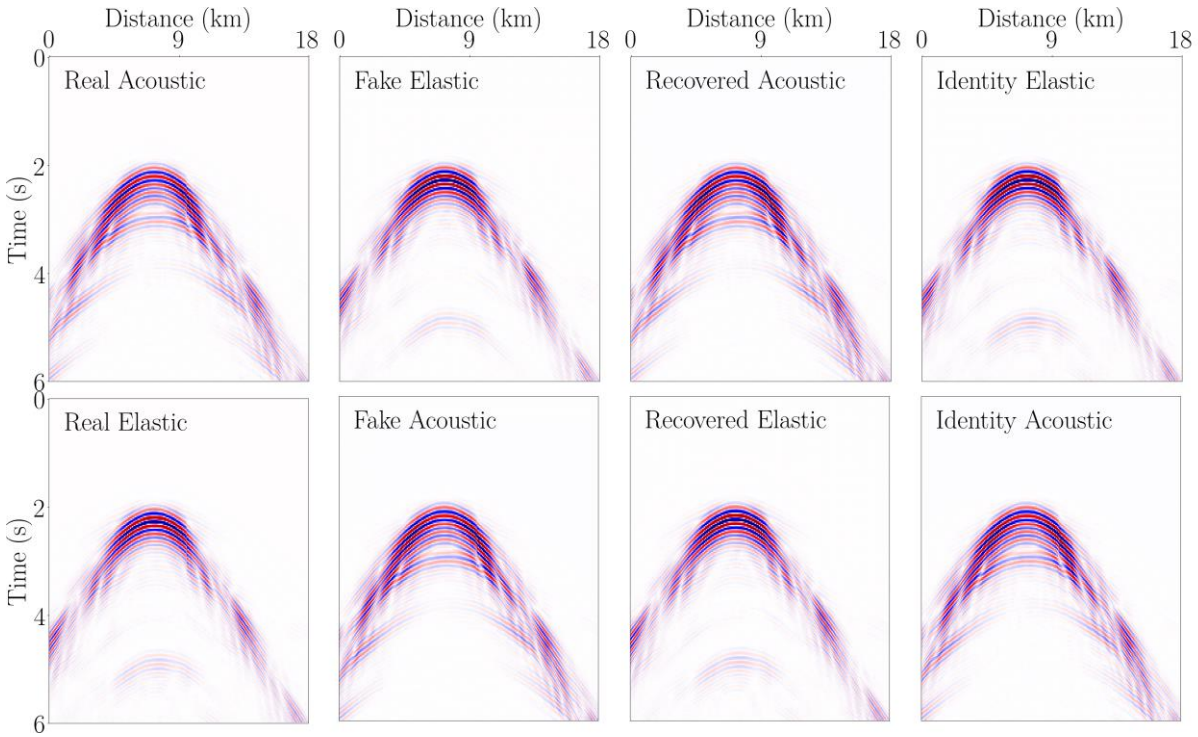

Figure 2 *A single shot record part way through the training process, at epoch 173.*

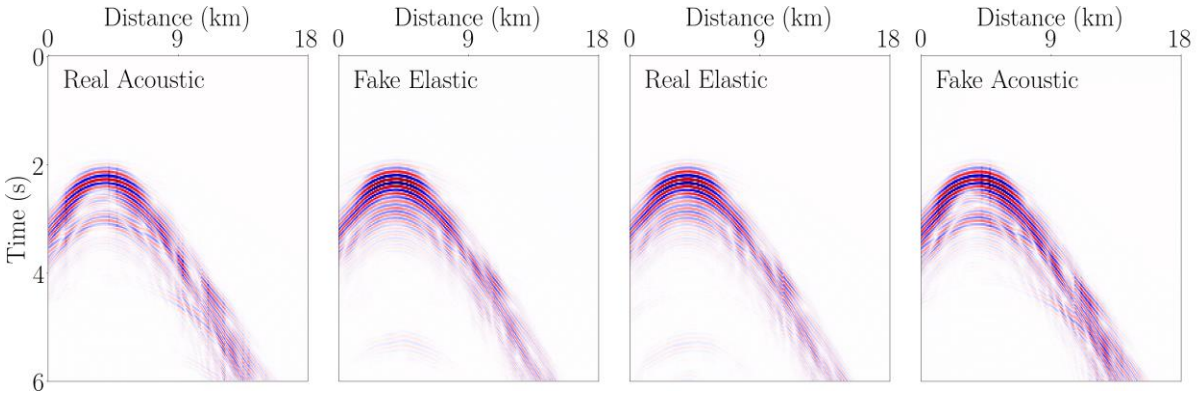

Figure 3 *Comparison between the real and fake data as generated by the two networks. The trained forward network removes the post-critical reflections and multiples from the real acoustic data, while the inverse network adds them into the real elastic data. In these results, the fake data match the real data at an average trace-by-trace L_2 error of 4.9%.*

Figure 3 shows the output of the fully trained networks applied to a synthetic shot record that was not included in the training set. The strong top-chalk reflections and their associated multiples present in the acoustic data have been successfully removed in the fake elastic data, and the fake datasets closely match their real equivalents. This means that the supervised CycleGAN is capable of producing accurate elastic shot records using only acoustic modelling, and therefore acts as a low-cost generator of elastic data. Note however, that fully elastic FWI requires not only elastic shot records but also the generation and storage of the forward elastic wavefield. In principle, the approach that we have used here would be capable of building such a forward wavefield, but its size and the volume of training required to build it in 3D is likely to be prohibitive, so that we follow a different route to low-cost inversion of elastic data here.

Figure 4 shows the results of the networks applied to a 2D slice through a 3D shot record for both synthetic and field data. The acoustic synthetic data can be used to produce fake elastic predicted data that can then be used to generate elastic residuals for FWI. And the elastic field data can be used to produce fake acoustic observed data that can be used as input to pure acoustic FWI. The fake acoustic data data in this figure appear plausible, but there is no way to test their accuracy directly since we do not of course have access to field data that is purely acoustic.

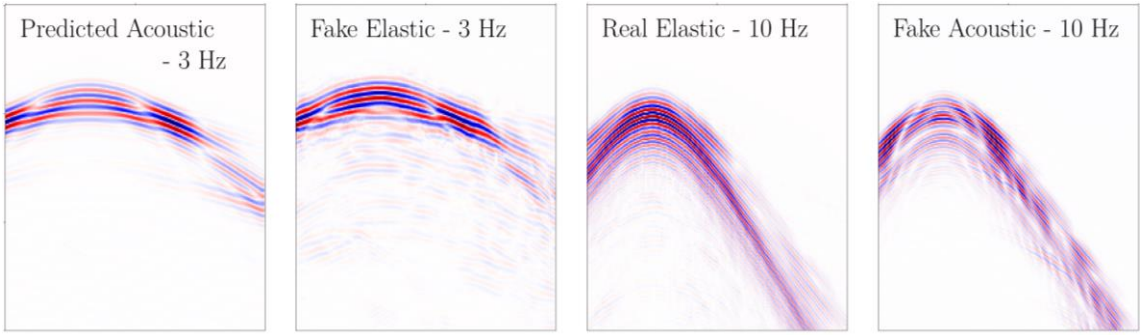

Figure 4 *From left to right: predicted acoustic data at 3 Hz and its fake elastic equivalent, elastic field data at 10 Hz and its fake acoustic equivalent.*

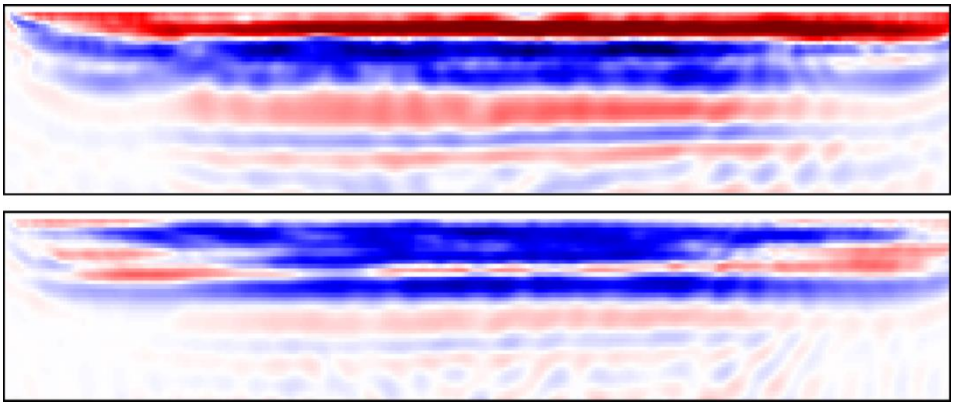

Figure 5 *Acoustic FWI gradients after a single iteration at 3 Hz using a smoothed starting model. The upper gradient is for FWI using the raw field data; the lower gradient is for FWI using the same data after processing by the trained network to generate fake acoustic field data.*

Figure 5 shows two raw FWI gradients: the upper one is for the raw field data and the lower is for the acoustic data generated by the network. The gradient is unscaled and has no spatial preconditioning or inverse Hessian applied. The problematic removal of the chalk layer during acoustic FWI is produced by the strong red region halfway down the top figure; this effect is absent in the lower gradient which instead acts to sharpen the previously smoothed top of chalk. The initial indications therefore are that the network-processed field data do not show the detrimental effects of elastic conversions at top chalk, and the gradient appears to be doing what we should expect at top chalk.

We have not yet inverted these data to completion. It is unclear at present whether it will prove to be necessary to retrain the network every iteration, or only after an increase in iteration frequency, or perhaps not at all. We have also not yet inverted fake elastic residuals – we intend to do this using acoustic forward and adjoint wave equations, but using the elastic residuals to form the adjoint source. This is not theoretically correct, but the history of practical FWI has been that acoustic FWI, with many short cuts and heuristics, fails in theory and only works in practice. We are hopeful that network-processing of predicted and/or observed data to change its apparent physics will follow the same rule. By the date of the workshop, we will have completed these tests, and so be in a stronger position to answer that question.

The approach that we have used here, changing the effective physics of a synthetic or field dataset, will have applications across many areas – some focused on reduced cost and others focused on improved outcomes. FWI appears to be a sensible place to begin this investigation because it is reasonably well understood, but the simulation of some types of physics is extremely expensive.

Acknowledgements

We thank CNOOC International and their partners for permission to publish this work.

References

He, K., Zhang, X., Ren, S. and Sun, J. [2016] Deep residual learning for image recognition. In: *Proceedings of the IEEE conference on computer vision and pattern recognition, 770–778.*

Hoffman, J., Tzeng, E., Park, T., Zh, J.Y., Isola, P., Saenko, K., Efros, A.A. and Darrell, T. [2017] Cycada: Cycle-consistent adversarial domain adaptation. *arXiv preprint arXiv:1711.03213.*

Zhu, J.Y., Park, T., Isola, P. and Efros, A.A. [2017] Unpaired image-to-image translation using cycle-consistent adversarial networks. *arXiv preprint.*